Non-local Restoration of Sparse 3D Single-Photon Data

NON-LOCAL RESTORATION OF SPARSE 3D SINGLE-PHOTON DATA

Songmao Chen[1,2,3], *Abderrahim Halimi*[3], *Ximing Ren*[3], *Aongus McCarthy*[3], *Xiuqin Su*[1,2], *Gerald S. Buller*[3], *Steve McLaughlin*[3]

(1) Institute of Optics and Precision Mechanics, Chinese Academy of Science, Xi'an, China
(2) University of Chinese Academy of Science (UCAS), Beijing, 100049, China
(3) School of Engineering and Physical Sciences, Heriot-Watt University, Edinburgh U.K.

ABSTRACT

This paper presents a new algorithm for the non-local restoration of single-photon 3-Dimensional Lidar images acquired in the photon starved regime or with a reduced number of scanned spatial points (pixels). The algorithm alternates between two steps: evaluation of the spatial correlations between pixels using a graph, then restore the depth and reflectivity images by their spatial correlations. To reduce the computational cost associated with the graph, we adopt a non-uniform sampling approach, where bigger patches are assigned to homogeneous regions and smaller ones to heterogeneous regions. The restoration of 3D images is achieved by minimizing a cost function accounting for the data Poisson statistics and the non-local spatial correlations between patches. This minimization problem is efficiently solved using the alternating direction method of multipliers (ADMM) that presents fast convergence properties. Results on real Lidar data show the benefits of the proposed algorithm in improving the quality of the estimated depth images, especially in photon starved cases, which can contain a reduced number of photons.

Index Terms— 3D Lidar imaging, image restoration, Poisson statistics, graph, non-uniform sampling.

1. INDRODUCTION

Imaging and sensing using the time-correlated single-photon counting approach have emerged as a candidate technology for a number of application areas including long distance imaging [1,2] and imaging in highly turbid media [3]. A single-photon Lidar system operates by directing laser pulses towards a target, detecting the scattered photons using single-photon avalanche diode (SPAD) detector and estimating the time-of-flight (TOF). A waveform is then formed via a histogram of the detected photons with respect to their TOF for each pixel, where the amplitude of the waveform peak represents the target reflectivity, and its time delay is the round-trip duration, and hence target distance. Above information form 3D image of the target. Of particular interest in real world applications is the photon starved case in which only a few photons are captured in each pixel location. The latter scenario occurs for long-range imaging or when reducing the acquisition time for rapid frame-rates. This paper is interested in the restoration of the 3D images in this scenario.

Several methods have been proposed in the literature to achieve this task, where most of them use similar ingredients. First, given the nature of the data, common Gaussian-based techniques lead to reduced restoration performance which promotes the design of specialized algorithms accounting for data statistics, e.g., binomial statistics [4, 5], Poisson statistics [6–10]. Second, the extraction of depth and reflectivity images being an ill-posed inverse problem, it is necessary to include prior knowledge or regularization to improve the quality of the estimates. This is often achieved by exploiting the redundant information in the data by accounting for correlations or by assuming sparsity in a transformed domain. Indeed, local approaches assume spatial correlations between adjacent pixels [11, 12] while most state-of-the-art algorithms extend this notion to non-local regions [6, 13, 14]. It is also common to assume the sparsity of the images in a transformed space, e.g., DCT or wavelet domain [15–18]. The third point exploits the multi-resolution information available in the data by using larger spatial points such as patches or superpixels [13, 19, 20] to build robust algorithms and reduce their sensitivity to pixel fluctuations due to noise or other corruptions. The proposed algorithm combines these ingredients to provide an efficient solution for 3D imaging using Lidar.

The first contribution of this paper is the use of a graph-based strategy to restore 3D Lidar data acquired under the photon starved regime. The first motivation for this choice is that it allows the use of a non-local approach to restore depth and reflectivity images. A second motivation is related to the possibility of acquiring Lidar data on a non-uniform grid, thus complex scenarios can be sensed intelligently and its spatial correlations can be efficiently learned by using the proposed graph approach. Furthermore, the correlations can be learned from other modalities (i.e. data from other sensors) when building the non-uniform patches. To reduce the computational cost when dealing with large graphs, the proposed method builds the graph on a patch-based non-uniform sampling grid which is scene dependent. In addition, the method exploits multi-resolution Lidar data to deliver robust estimation performance. The second contribution is related to the restoration of depth and reflectivity images using the learned spatial correlations. The images are divided into regions according to their affinity and the pixels of each region are then restored by minmizing a cost function accounting for their Poisson statistics and learned spatial correlations [21, 22]. The minimization is approximated using an alternating direction method of multipliers (ADMM) [23]. More precisely, the ADMM variant proposed in [24, 25] was adopted to solve the optimization problem, as it is fast and shows good convergence properties. The proposed approach is validated on real field data showing improved depth estimates especially when reducing the photon counts.

The paper is organized as follows. Section 2 introduces the statistical model associated with the observed photon counts and the adopted assumptions. Section 3 presents the proposed approach

This work was supported by the EPSRC Grants EP/J015180/1, EP/N003446/1, EP/M01326X/1, and the UK Royal Academy of Engineering under the Research Fellowship Scheme (RF/201718/17128). S. Chen is supported by China Scholarship Council (CSC) joint PhD Training Program.

based on learning spatial correlations and parameter restoration. Section 4 describes the considered ADMM algorithm for parameter estimation. Results on real data are provided in Section 5. Finally, conclusions and future work are discussed in Section 6.

2. PROBLEM FORMULATION

Let $\boldsymbol{y}_{i,j,t}$ be the Lidar observation which denotes the number of observed photon counts within the tth bin of the pixel (i,j), where $(i,j) \in \{1,\cdots,N_r\} \times \{1,\cdots,N_c\}$, and $\boldsymbol{Y}$ be a cube of size $N_r \times N_c \times T$ gathering all observations where T is the total number of bins, and bin is the minimum interval in timing module. Based on [26, 27], we assume the observed photon counts $\boldsymbol{y}_{i,j,t}$ are drawn from Poisson distribution which interpreted as follow

$$y_{i,j,t} \sim \mathcal{P}\left(s_{i,j,t}\right) \tag{1}$$

where

$$s_{i,j,t} = r_{i,j} f\left(t - t_{i,j}\right) + b_{i,j} \tag{2}$$

and $r_{i,j} \geq 0$ stands for the reflectivity of the target, $t_{i,j} \geq 0$ represents the time-of-flight related to the range of the target, $b_{i,j} \geq 0$ is a constant for all bins denoting the background and dark photon level, and f denotes the system impulse response assumed to be known from the calibration step. Moreover, as $t_{i,j}$ is linearly related to the target depth, it is considered to be depth in this paper. The proposed algorithm aims to restore $r_{i,j}$ and $t_{i,j}$ in the photon starved case by considering the data statistics and spatially non-local smoothness constraints obtained on depth and reflectivity (DR) images. Furthermore, let $\boldsymbol{z}$ be a $2N \times 1$ vector where $\boldsymbol{z} = [\boldsymbol{z}_1^T, \boldsymbol{z}_2^T]^T = [\boldsymbol{t}^T, \boldsymbol{r}^T]^T$ gathers all $t_{i,j}, r_{i,j}$ and $N = N_r \times N_c$ is the number of pixels, where both $\boldsymbol{t}$ and $\boldsymbol{r}$ are $N \times 1$ vectors. The goal is to estimate depth and reflectivity images when receiving a reduced number of photons due to a fast acquisition or kilometre range imaging. In this case, a common maximum likelihood estimation strategy will lead to noisy estimates, hence the need for a restoration algorithm. In this paper, we adopt common assumptions to simplify the obtained formulation. First, similar to classical estimation approach, we assume the absence of the background level (i.e. $b_{i,j} = 0$) which is valid when taking measurements in dark conditions (e.g., night or laboratory measurements). Second, we assume that the observation window covers the entire object depth, in which case the sum of instrument pulse response is a constant $c_f = \sum_{t=1}^{T} f(t - t_{i,j}), \forall (i,j)$ for all pixels (i.e., a narrow peak that is generally located in the centre of the interval $[0, T]$).

3. PROPOSED APPROACH

The proposed algorithm restores the parameters by exploiting the spatial correlations between pixels. It iterates between two main steps: learning spatial correlations between non-uniformly sampled patches (or spatial locations), and use these correlations to restore the estimates. Both steps are described in the next subsections.

3.1. Learning correlations

This section aims to learn the correlations between the image elements in order to use them in the next restoration step. Note that the spatial correlations are learned from the 2D images $\boldsymbol{t}$ and $\boldsymbol{r}$ instead of the original 3D cube to avoid manipulation of large volume of data. However, this choice requires clean versions of these two images especially during initialization where $\boldsymbol{t}$, $\boldsymbol{r}$ might be too corrupted. To provide better initialization of $\boldsymbol{t}$ and $\boldsymbol{r}$ images, this papers exploit the information obtained from low-pass filtered histograms [5, 10]. Indeed, spatial low-resolution histograms present a better signal-to-background ratio and will be used to provide cleaner initial $\boldsymbol{t}$ and $\boldsymbol{r}$ images by replacing their missing pixels (i.e. pixels with no detected photons) and noisy pixels. It is important to extend local based restoration approaches [11, 12] to exploit non-local correlations as adopted in most state-of-the-art image restoration algorithms [6, 13, 14]. In this paper, we use a graph based approach to learn such correlations from the observed scene and use them to perform parameter restoration in the next section. Assume a vector of nodes $\boldsymbol{a}$ of size $N_p \times 1$, correlations between nodes are often evaluated in an $N_p \times N_p$ graph $\boldsymbol{W}$ with positive elements ($w_{ij} > 0$) representing the degree of similarity between nodes a_i and a_j. Different heuristic can be chosen to evaluate $\boldsymbol{W}$, for example, Gaussian kernel is applied in this paper as follow

$$w_{i,j} = \exp\left[-\frac{||a_i - a_j||^2}{2\sigma^2}\right] \tag{3}$$

where the scaling parameter σ is the kernel's bandwidth, and $||.||$ stands for ℓ_2 norm such that $||\boldsymbol{x}||^2 = \boldsymbol{x}^T\boldsymbol{x}$. The definition of the nodes will directly affect the performance of the algorithm in terms of estimation quality and computational cost. We choose the nodes as a weighted sum of normalized depth and reflectivity images. Note that one can also choose to include the observed data histograms in the nodes definition as in [28], but we prefer here to only consider the parameters that are iteratively restored using the proposed algorithm to learn better correlations. Associating each node with one pixel of the image leads to a huge affinity graph which prevents its use for real world applications (an $N = 128 \times 128$ image leads to a graph of size $N \times N = 16384 \times 16384$). To reduce the number of nodes, a solution is to associate a node with a pixel of a downsampled image, i.e., a patch of pixels. Uniform down-sampling allows to save computational cost, however, it does not account for the shape of the observed scene. A non-uniform sampling is proposed here with flexible patch sizes by giving homogeneous regions smaller sized patches and bigger sized patches to smooth areas, i.e., a scene dependent sampling. The procedure begins from a coarse image of features with uniform patches of size $2^{L-1} \times 2^{L-1}$ and proceed by dividing a patch if it contains heterogeneous information and keeping it if it is smooth. This is an iterative procedure where the patch sizes at step 1 are $2^{L-1} \times 2^{L-1}$, at step 2 they are $2^{L-2} \times 2^{L-2}$ for heterogeous patches, and they might reach $2^{L-\ell} \times 2^{L-\ell}$ at step ℓ for heterogeous patches. More precisely, the procedure is based on three steps:

(i) Apply a binary edge detection on the fine resolution feature image. This is performed using a gradient computation and thresholding at the pixel level (the thresholds are selected by the user given physical considerations, e.g., the depth threshold can be fixed to 1 mm),

(ii) Begin the iteration procedure by averaging the binary values of current patches (from the coarse image)

(iii) Divide patches if their value is higher than a user given threshold. Repeat (ii) and (iii) until stopping criteria.

This procedure leads to a scene dependent non-uniform sampling. Note that the procedure is terminated when reaching the finest level (i.e., patches of size 1×1), or when reaching a user defined maximum number of patches. The latter simulates the case where we only have limited memory to only account for a given number of patches, i.e., a limited number of sampling points. To further reduce complexity, algorithm [29] is applied to the resulting graph to partition its nodes into K sub-graphs or clusters. The patches of each sub-

graph can then be restored independently in the next section, which is of great interest to reduce the computational cost.

3.2. Parameter restoration

This section restores the depth $\boldsymbol{t}$ and reflectivity $\boldsymbol{r}$ images due to the photon starved regime, by considering the data statistics and prior knowledge introduced by regularization term. Let $\mathcal{C}(.)$ be the cost function, $\rho(.)$ be the negative log-likelihood derived from the data Poisson statistics and $\phi(.)$ be the regularization term. The cost function can be given as follows

$$\mathcal{C}(\boldsymbol{t},\boldsymbol{r}) = \rho(\boldsymbol{M}\boldsymbol{t},\boldsymbol{M}\boldsymbol{r}) + \phi(\boldsymbol{t},\boldsymbol{r}) \tag{4}$$

where $\boldsymbol{M}$ is an $E\times N$ binary mask that picks the E non-empty pixels by having one non-zero element in each row. It satisfies $\boldsymbol{M}\boldsymbol{M}^T = \mathbb{I}_E$ due to its particular structure, where $\mathbb{I}_E$ is the $E \times E$ identity matrix. This removes the empty pixels from the likelihood term, and reconstructs them using the prior knowledge.

3.2.1. Likelihood

From equations (1) and (2), the joint likelihood is obtained by assuming independence between the observed pixels

$$P(\boldsymbol{Y}|\boldsymbol{t},\boldsymbol{r},\boldsymbol{b}) = \prod_{i,j}\prod_{t=1}^{T} \frac{s_{i,j,t}^{y_{i,j,t}}}{y_{i,j,t}!}\exp^{-s_{i,j,t}} \tag{5}$$

where $\boldsymbol{r},\boldsymbol{t}$ are $N\times 1$ vectors gathering the elements $r_{i,j}, t_{i,j}, \forall i, \forall j$ (in lexicographic order). Given (5) and the adopted assumptions in Section 2, the negative log-likelihood is given by

$$\rho(\boldsymbol{t},\boldsymbol{r}) = -\log\left[P(\boldsymbol{Y}|\boldsymbol{t},\boldsymbol{r},\boldsymbol{b})\right] = \sum_{ij}\rho_{i,j} + cst \tag{6}$$

where cst represents unnecessary constants and

$$\begin{aligned}\rho_{i,j} &= c_f r_{i,j} + i_{\mathbb{R}_+}(r_{i,j},t_{i,j}) \\ &\quad -\sum_{t=1}^{T} y_{i,j,t}\left\{\log\left(r_{i,j}\right) + \log[f(t-t_{i,j})]\right\}\end{aligned} \tag{7}$$

where $i_{\mathbb{R}_+}(.)$ is the indicator function imposing non-negativity. It is important to note that the estimation is performed on the adaptive sized patches, where the histogram of each patch is the sum of the pixels within the patch. Furthermore, the likelihood is separable w.r.t $r_{i,j}$ and $t_{i,j}$ which can be processed independently. Such advantages will be illustrated in subsequent sections.

3.2.2. Prior

Akin to [30], we assume a centred multivariate Gaussian prior distribution for the pixels of depth $\boldsymbol{t}_k$ and reflectivity $\boldsymbol{r}_k$ images belonging to the k-th cluster, where the correlations learned in Section 3.1 are introduced through the covariance matrices. Straightforward computations lead to the following negative log-prior or Laplacian regularization

$$\phi(\boldsymbol{t}_k,\boldsymbol{r}_k) = \sigma_1\boldsymbol{t}_k^T\boldsymbol{P}^k\boldsymbol{t}_k + \sigma_2\boldsymbol{r}_k^T\boldsymbol{P}^k\boldsymbol{r}_k \tag{8}$$

where σ_1 and σ_2 control the degree of regularization, $\boldsymbol{P}^k = \boldsymbol{Q}^k - \boldsymbol{W}^k$ is the graph Laplacian matrix of the k-th cluster in which $\boldsymbol{Q}^k_{ii} = \sum_{j=1}^{N} w^k_{ij}$ is a diagonal matrix and $\boldsymbol{W}^k$ is the affinity graph of the pixels belonging to the k-th cluster. According to (4), the cost function of the k-th cluster can be written as follows

$$\mathcal{C}(\boldsymbol{t}_k,\boldsymbol{r}_k) = \rho(\boldsymbol{M}_k\boldsymbol{t}_k,\boldsymbol{M}_k\boldsymbol{r}_k) + \sigma_1\boldsymbol{t}_k^T\boldsymbol{P}^k\boldsymbol{t}_k + \sigma_2\boldsymbol{r}_k^T\boldsymbol{P}^k\boldsymbol{r}_k \tag{9}$$

where $\boldsymbol{M}_k$ is obtained by selecting the columns of $\boldsymbol{M}$ corresponding to the pixels/patches in k-th cluster. Finally, it is clear from (9), each cluster k will be restored independently from the others. Therefore, we drop the index "k" in the following for brevity.

4. ESTIMATION ALGORITHM

This section describes the alternating direction method of multipliers (ADMM) [31] used to minimize the cost function (9). The main idea of ADMM algorithm is to divide the formulation into a set of simple sub problems that are easy to solve. This section first introduces a generalized formulation of a variant of the ADMM algorithm [25], then demonstrates its use in our case.

4.1. General formulation

Consider the generalized optimization problem which contains J sub problems

$$\underset{\boldsymbol{z}}{\operatorname{argmin}}\, \mathcal{C}\left(\boldsymbol{z}\right) = \underset{\boldsymbol{z}}{\operatorname{argmin}} \sum_{j=1}^{J} g_j\left(\boldsymbol{H}^{(j)}\boldsymbol{z}\right) \tag{10}$$

where $\boldsymbol{z}\in\mathbb{R}^d$, $g_j : \mathbb{R}^{p_j}\rightarrow\mathbb{R}$ are closed, proper, convex functions, and $\boldsymbol{H}^{(j)} \in \mathbb{R}^{p_j\times d}$ are arbitrary matrices. By denoting $\boldsymbol{u}^{(j)} = \boldsymbol{H}^{(j)}\boldsymbol{z} \in \mathbb{R}^{p_j}$ and $\boldsymbol{d}^{(j)} \in \mathbb{R}^{p_j}$ which is introduced as an auxiliary vector, problem (10) can be solved using a variant of the ADMM algorithm proposed in [24] and summarized in Algo. 1.

Algorithm 1 ADMM variant for (10)

1: input: g_j, $\boldsymbol{H}^{(j)}, \forall j$
2: Initialize $\boldsymbol{z}, \boldsymbol{u}_0^{(j)}, \boldsymbol{d}_0^{(j)}, \forall j, \mu, \epsilon$
3: Set $i \leftarrow 0$, conv$\leftarrow 0$
4: **while** conv$= 0$ **do**
5: **for** j=1:J **do**
6: $\lambda_i^{(j)} \leftarrow \boldsymbol{u}_i^{(j)} + \boldsymbol{d}_i^{(j)}$,
7: **end for**
8: $\boldsymbol{z}_{i+1} \leftarrow \boldsymbol{X}^{-1}\sum_{j=1}^{J}\left(\boldsymbol{H}^{(j)}\right)^{\top}\lambda_i^{(j)}$,
9: **for** j=1:J **do**
10: $\boldsymbol{v}_i^{(j)} \leftarrow \boldsymbol{H}^{(j)}\boldsymbol{z}_{i+1} - \boldsymbol{d}_i^{(j)}$,
11: $\boldsymbol{u}_{i+1}^{(j)} \leftarrow \underset{\boldsymbol{s}}{\operatorname{argmin}}\, \frac{\mu}{2}||\boldsymbol{s} - \boldsymbol{v}_i^{(j)}||^2 + g_j\left(\boldsymbol{s}\right)$,
12: $\boldsymbol{d}_{i+1}^{(j)} \leftarrow \boldsymbol{d}_i^{(j)} - \left(\boldsymbol{H}^{(j)}\boldsymbol{z}_{i+1} - \boldsymbol{u}_{i+1}^{(j)}\right)$,
13: **end for**
14: $i = i+1$
15: **if** $||\boldsymbol{z}_{i+1} - \boldsymbol{z}_i|| < \epsilon$ **then**
16: conv$\leftarrow 1$
17: **end if**
18: **end while**
19: output: $\boldsymbol{z}_{i+1}$

This algorithm convergence is guaranteed when the matrix $\boldsymbol{X} = \left[\sum_{j=1}^{J}\left(\boldsymbol{H}^{(j)}\right)^{\top}\boldsymbol{H}^{(j)}\right]$ has full rank, the g_j are closed, proper, convex functions, and the proximity term in line 11 are solved exactly or if their sequences of errors are absolutely summable. Note that μ stands for the Lagrange multiplier and ϵ is the stopping threshold.

4.2. Restoration

Considering the $2N_p^k \times 1$ vector $\boldsymbol{z} = [\boldsymbol{t}^T, \boldsymbol{r}^T]^T = [\boldsymbol{z}_1^T, \boldsymbol{z}_2^T]^T$, problem (9) can be divided into 4 sub-problems

$$g_1\left(\boldsymbol{u}_i^{(1)}\right) = c_f \boldsymbol{u}_i^{(1)} - \sum_{t=1}^{T} y_{i,j,t} \log\left(u_i^{(1)}\right), \quad \boldsymbol{H}^{(1)} = [\boldsymbol{0}_{N_p^k}, \boldsymbol{M}]$$

$$g_2\left(\boldsymbol{u}_i^{(2)}\right) = -\sum_{t=1}^{T} y_{i,j,t} \log\left[f(t - u_i^{(2)})\right], \quad \boldsymbol{H}^{(2)} = [\boldsymbol{M}, \boldsymbol{0}_{N_p^k}]$$

$$g_3\left(\boldsymbol{u}^{(3)}\right) = \sigma_1 \boldsymbol{z}_1^T \boldsymbol{P} \boldsymbol{z}_1 + \sigma_2 \boldsymbol{z}_2^T \boldsymbol{P} \boldsymbol{z}_2, \quad \boldsymbol{H}^{(3)} = \mathbb{I}_{2N_p^k}$$

$$g_4\left(\boldsymbol{u}^{(4)}\right) = i_{\mathrm{R}_+^{N_p^k}}\left(\boldsymbol{u}^{(4)}\right), \quad \boldsymbol{H}^{(4)} = \mathbb{I}_{2N_p^k}$$

where $2N_p^k$ is the number of nodes in the kth cluster, $\boldsymbol{u}^{(3)} = \boldsymbol{z}$ and $\boldsymbol{X}$ simplifies to a full rank diagonal matrix (fast to inverse) due to the unique structure of $\boldsymbol{H}^{(j)}, \forall j \in \{1, \cdots, J\}$. The optimization problems in line 11 are straightforward for $j = 1$ and 3 which have analytical solutions. Variable $u_i^{(2)}$ is updated by solving a discrete optimization problem. It is solved by visiting every potential solution ($u_i^{(2)} \in (0, T]$) as the number of bins T is a finite number (usually an acceptable size). Although the convexity of g_2 is not guaranteed, the ADMM algorithm shows good convergence in practice. Note this can be improved by reducing the searching space using the prior information from low-pass filtered histograms.

5. RESULTS ON REAL DATA

This section considers six real images (128×128 pixels) of a life-sized white polystyrene head, acquired at a distance of 40m in the Edinburgh Campus of Heriot-Watt University, using a Lidar system based on time correlated single-photon counting (TCSPC) [27, 32, 33]. The acquisition time is 30ms per-pixel, but given the time tagged detection, it is possible to simulate a reduction in acquisition time to obtain 60μs, 300μs, 600μs, 3ms, 6ms and 30ms which correspond to an average photon-per-pixel (ppp) levels of 0.80, 4.09, 8.21, 41.06, 82.02, 410.00. The proposed algorithm is compared with the classical cross-correlation approach (maximum likelihood approach in absence of background noise), RDI-TV [15] that assumes local-correlations and has previously shown good performance compared to BM3D [13], and the unmixing algorithm [5] (UA) which is the state-of-the-art-algorithm to restore single-layer 3D Lidar data.

Table 1. Depth and reflectivity SRE results for different algorithms and acquisition times under full resolution (Proposed algorithm works under 4096 non-uniform patches).

Acquistion time (ms)		0.06	0.3	0.6	3	6
Depth	Proposed	29.8	**32.9**	34.3	35.1	36.1
	RDI-TV	28.9	32.0	**35.0**	**35.8**	**37.0**
	UA	**29.9**	32.3	33.7	35.1	36.4
Reflect.	Proposed	**5.4**	8.1	8.5	8.7	8.8
	RDI-TV	1.7	**9.0**	**10.0**	10.7	10.9
	UA	3.6	6.6	8.5	**10.8**	**11.4**

To highlight the benefit of the non-uniform sampling, we assume that we only acquire 4096 spatial points, which will be scene dependent for the proposed algorithm, and full resolution (128×128 pixels $=$ 16384 pixels) for the other considered algorithms. Fig. 1 shows the depth results obtained by different methods. This figure highlights the benefit of the proposed algorithm in comparison with UA and RDI-TV. Quantitative results are also provided in Table. 1 showing better depth and reflectivity signal-to-reconstruction-error (SRE) results for the proposed approach, where SRE $= 10\log_{10}\left(\frac{||\boldsymbol{x}||^2}{||\boldsymbol{x}-\widehat{\boldsymbol{x}}||^2}\right)$, $\boldsymbol{x}$ is the reference depth or reflectivity images obtained from 30ms data, and $\widehat{\boldsymbol{x}}$ is the restored image. Table. 2 also illustrates the fast performance of the proposed algorithm when compared to RDI-TV. Further time improvement can be obtained by adopting a parallelisation approach as for UA. In summary, the proposed algorithm takes medium processing time and showed best performance in the photon starved case. For higher acquisition time cases, similar performance were obtained compared to other methods.

Table 2. Processing time of different algorithms (in seconds). Proposed algorithm uses 4096 patches. RDI-TV and UA use full resolution (16384 pixels).

Acquistion time (ms)	0.06	0.3	0.6	3	6
Proposed	10.80	9.68	7.23	6.44	6.26
RDI-TV	19.45	13.15	11.73	11.38	9.38
UA	5.73	4.48	4.36	4.06	4.11

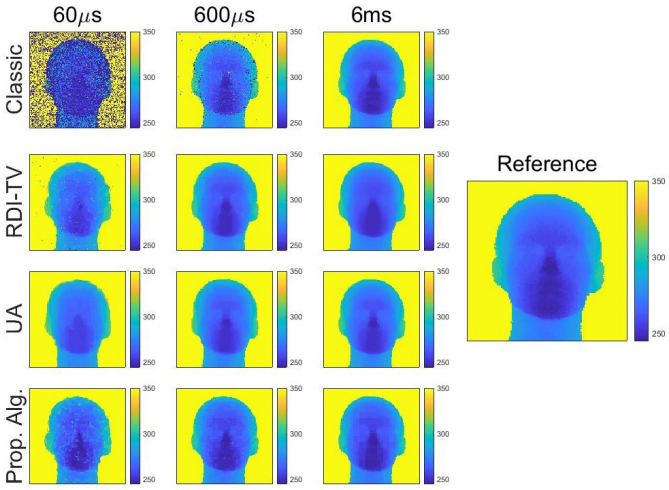

Fig. 1. Depth maps obtained by different methods on Mannequin face. Columns from left to right corresponds to data of different acquisition time i.e., 60μs, 600μs, 6ms and reference image. Rows from top to bottom corresponds to different methods i.e. cross-correlation, RDI-TV, UA and proposed algorithm

6. CONCLUSIONS

This paper presented a new formulation for the joint restoration of depth and reflectivity images in photon-starved regime. The proposed framework first use a coarse-to-fine strategy to obtain a good parameter initialization by exploiting the information of different resolutions, then learn the spatial correlation by using a non-local graph based approach, afterwards restore depth and reflectivity images by considering data statistics and spatial correlations. Efforts to improve the robustness have been made by extracting features

that combine depth and reflectivity information. Furthermore, non-uniform sampling was proposed to reduce the computational cost while preserving the useful information, which improve the results. The simplified formulation reduce to a sum of sub functions with respect to parameters of interest, which is efficiently solved by an alternating direction method of multipliers algorithm. The proposed framework and formulation shows superior performance on sparse real data when compared to different algorithms. Future work include the study of other regularization terms for depth and reflectivity images. Considering adaptive sampling to achieve smart imaging is interesting and will be investigated in the future.

7. REFERENCES

[1] A. M. Pawlikowska, A. Halimi, R. A. Lamb, and G. S. Buller, "Single-photon three-dimensional imaging at up to 10 kilometers range," *Opt. Eng*, vol. 25, no. 10, pp. 11 919–11 931, 2017.

[2] R. Tobin, A. Halimi, A.McCarthy, X. Ren, K. J. McEwan, S. McLaughlin, and G. S. Buller, "Long-range depth profiling of camouflaged targets using single-photon detection," *Opt. Eng*, vol. 57, no. 3, p. 031303, 2017.

[3] A. Halimi, A. Maccarone, A. McCarthy, S. McLaughlin, and G. S. Buller, "Object depth profile and reflectivity restoration from sparse single-photon data acquired in underwater environments," *IEEE Trans. Comput. Imaging*, vol. 3, no. 3, pp. 472–484, 2017.

[4] X. Ren, P. W. R. Connolly, A. Halimi, Y. Altmann, S. McLaughlin, I. Gyongy, R. K. Henderson, and G. S. Buller, "High-resolution depth profiling using a range-gated cmos spad quanta image sensor," *Opt. Express*, vol. 26, no. 5, pp. 5541–5557, Mar 2018.

[5] J. Rapp and V. K. Goyal, "A few photons among many: Unmixing signal andnoise for photon-efficient active imaging," *IEEE Trans. Comput. Imaging*, vol. 3, no. 3, pp. 445–459, Sept. 2017.

[6] J. Salmon, Z. Harmany, C.-A. Deledalle, and R. Willett, "Poisson noise reduction with non-local PCA," *Journal of Mathematical Imaging and Vision*, vol. 48, no. 2, pp. 279–294, 2014.

[7] D. Shin, F. Xu, F. N. C. Wong, J. H. Shapiro, and V. K. Goyal, "Computational multi-depth single-photon imaging," *Opt. Express*, vol. 24, no. 3, pp. 1873–1888, Feb 2016.

[8] T. Remez, O. Litany, R. Giryes, and A. M. Bronstein, "Deep convolutional denoising of low-light images," in *ArXiv e-prints*, Jan. 2017.

[9] L. Azzari and A. Foi, "Variance stabilization for noisy+estimate combination in iterative poisson denoising," *IEEE Signal Processing Lett.*, vol. 23, no. 8, pp. 1086–1090, Aug 2016.

[10] W. Marais and R. Willett, "Proximal-gradient methods for poisson image reconstruction with bm3d-based regularization," in *2017 IEEE 7th International Workshop on Computational Advances in Multi-Sensor Adaptive Processing (CAMSAP)*, 2017, pp. 183–187.

[11] L. I. Rudin, S. Osher, and E. Fatemi, "Nonlinear total variation based noise removal algorithms," *Phys. D*, vol. 60, no. 1-4, pp. 259–268, Nov. 1992.

[12] S. Geman and D. Geman, "Stochastic relaxation, gibbs distributions, and the bayesian restoration of images," *IEEE Transactions on Pattern Analysis and Machine Intelligence*, vol. PAMI-6, no. 6, pp. 721–741, Nov 1984.

[13] K. Dabov, A. Foi, V. Katkovnik, and K. Egiazarian, "Image denoising by sparse 3-d transform-domain collaborative filtering," *IEEE Trans. Image Process.*, vol. 16, no. 8, pp. 2080–2095, Aug 2007.

[14] A. Buades, B. Coll, and J. M. Morel, "A review of image denoising algorithms, with a new one," *Multiscale Modeling & Simulation*, vol. 4, no. 2, pp. 490–530, 2005.

[15] A. Halimi, Y. Altmann, A. McCarthy, X. Ren, R. Tobin, G. S. Buller, and S. McLaughlin, "Restoration of intensity and depth images constructed by using sparse single-photon data," in *European Signal Processing Conf. (EUSIPCO)*, 2016, pp. 86–90.

[16] M. A. T. Figueiredo and R. D. Nowak, "An EM algorithm for wavelet-based image restoration," *IEEE Trans. Image Process.*, vol. 12, no. 8, pp. 906–916, Aug 2003.

[17] B. Zhang, J. M. Fadili, and J. Starck, "Wavelets, ridgelets, and curvelets for poisson noise removal," *IEEE Trans. Image Process.*, vol. 17, no. 7, pp. 1093–1108, July 2008.

[18] R. Yan, L. Shao, and Y. Liu, "Nonlocal hierarchical dictionary learning using wavelets for image denoising," *IEEE Trans. Image Process.*, vol. 22, no. 12, pp. 4689–4698, Dec 2013.

[19] M. V. den Bergh, D. Carton, and L. V. Gool, "Depth seeds: Recovering incomplete depth data using superpixels," in *2013 IEEE Workshop on Applications of Computer Vision (WACV)*, Jan 2013, pp. 363–368.

[20] Y. Liu, J. Bioucas-Dias, J. Li, and A. Plaza, "Multi-superpixelization-based convex formulation for joint classification of hyperspectral and lidar data," in *Proc. IEEE Int. Conf. Geosci. Remote Sens. (IGARSS)*, July 2017, pp. 807–810.

[21] B. Mohar and Y. Alavi, "The laplacian spectrum of graphs," *Graph theory, combinatorics, and applications*, vol. 57, no. 3, 1991.

[22] R. Ammanouil, A. Ferrari, and C. Richard, "A graph laplacian regularization for hyperspectral data unmixing," in *2015 IEEE International Conference on Acoustics, Speech and Signal Processing (ICASSP)*, April 2015, pp. 1637–1641.

[23] S. Boyd, N. Parikh, E. Chu, B. Peleato, and J. Eckstein, "Distributed optimization and statistical learning via the alternating direction method of multipliers," *Found. Trends Mach. Learn.*, vol. 3, no. 1, pp. 1–122, Jan 2011.

[24] M. Figueiredo and J. Bioucas-Dias, "Restoration of poissonian images using alternating direction optimization," *IEEE Trans. Image Process.*, vol. 19, no. 12, pp. 3133–3145, Dec 2010.

[25] M. Afonso, J. Bioucas-Dias, and M. Figueiredo, "An augmented lagrangian approach to the constrained optimization formulation of imaging inverse problems," *IEEE Trans. Image Process.*, vol. 20, no. 3, pp. 681–695, March 2011.

[26] S. Hernandez-Marin, A. Wallace, and G. Gibson, "Bayesian analysis of lidar signals with multiple returns," *IEEE Trans. Pattern Anal. Mach. Intell.*, vol. 29, no. 12, pp. 2170–2180, Dec. 2007.

[27] Y. Altmann, X. Ren, A. McCarthy, G. S. Buller, and S. McLaughlin, "Lidar waveform-based analysis of depth images constructed using sparse single-photon data," *IEEE Trans. Image Process.*, vol. 25, no. 5, pp. 1935–1946, May 2016.

[28] A. Halimi, P. Connolly, X. Ren, Y. Altmann, I. Gyongy, R. K. Henderson, S.McLaughlin, and G. S. Buller, "Restoration of depth and intensity images using a graph laplacian regularization," in *2017 IEEE 7th International Workshop on Computational Advances in Multi-Sensor Adaptive Processing (CAMSAP)*, 2017.

[29] A. Y. Ng, M. I. Jordan, and Y. Weiss, "On spectral clustering: Analysis and an algorithm," in *Advances in neural information process. systems*. MIT Press, 2001, pp. 849–856.

[30] A. Halimi, C. Mailhes, J.-Y. Tourneret, and H. Snoussi, "Bayesian estimation of smooth altimetric parameters: Application to conventional and delay/Doppler altimetry," *IEEE Trans. Geosci. Remote Sens.*, 2015, to appear.

[31] A. Halimi, J. Bioucas-Dias, N. Dobigeon, G. Buller, and S. McLaughlin, "Fast hyperspectral unmixing in presence of nonlinearity or mismodeling effects," *IEEE Trans. Comput. Imaging*, vol. 3, no. 2, pp. 146–159, 2017.

[32] A. McCarthy, X. Ren, A. D. Frera, N. R. Gemmell, N. J. Krichel, C. Scarcella, A. Ruggeri, A. Tosi, and G. S. Buller, "Kilometer-range depth imaging at 1550 nm wavelength using an InGaAs/InP single-photon avalanche diode detector," *Opt. Express*, vol. 21, no. 19, pp. 22 098–22 113, Sep 2013.

[33] A. M. Wallace, J. Ye, N. Krichel, A. McCarthy, R. Collins, and G. S. Buller, "Full waveform analysis for long-range 3d imaging laser radar," *EURASIP Journal on Advances in Signal Process.*, vol. 2010, p. 896708, Dec. 2010.